Journal of Radiation Research Advance Access published February 5, 2013

Journal of Radiation Research, 2013, pp 1–17
doi: 10.1093/jrr/rrs124

Facility optimization to improve activation rate distributions during IVNAA

Atiyeh EBRAHIMI KHANKOOK, Laleh RAFAT MOTAVALLI and Hashem MIRI HAKIMABAD*

Physics Department, College of Sciences, Ferdowsi University of Mashhad, 91775-1436, Mashhad, Iran
*Corresponding author. Tel: +98-511-8797022; Fax: +98-511-8796416; E-mail: mirihakim@ferdowsi.um.ac.ir; mirihakim@yahoo.com

(Received 19 November 2011; revised 2 October 2012; accepted 26 November 2012)

Currently, determination of body composition is the most useful method for distinguishing between certain diseases. The prompt-gamma *in vivo* neutron activation analysis (IVNAA) facility for non-destructive elemental analysis of the human body is the gold standard method for this type of analysis. In order to obtain accurate measurements using the IVNAA system, the activation probability in the body must be uniform. This can be difficult to achieve, as body shape and body composition affect the rate of activation. The aim of this study was to determine the optimum pre-moderator, in terms of material for attaining uniform activation probability with a CV value of about 10% and changing the collimator role to increase activation rate within the body. Such uniformity was obtained with a high thickness of paraffin pre-moderator, however, because of increasing secondary photon flux received by the detectors it was not an appropriate choice. Our final calculations indicated that using two paraffin slabs with a thickness of 3 cm as a pre-moderator, in the presence of 2 cm Bi on the collimator, achieves a satisfactory distribution of activation rate in the body.

Keywords: activation rate; neutron flux uniformity; MCNP; IVNAA; pre-moderator; collimator

INTRODUCTION

The *in vivo* neutron activation analysis method (IVNAA) provides an elemental profile of body composition that is independent of the molecular or chemical structure of the tissue. With the neutron activation method, the sample is bombarded with neutrons; consequently, the radioactive isotopes that emit the characteristic gamma rays will be formed. Comparison of the intensity of these gamma rays with those emitted by a standard permits a quantitative measure of the concentrations of the various nuclides [1].

In 1964 Anderson *et al.* showed that neutron activation analysis could be applied to the measurement of total body elements [2]. The clinical and biological application of the neutron activation method has since been actively pursued for over four decades. However, a basic problem with this technique is obtaining uniformity of neutron activation probability in the body [3, 4]. Neutron activation probability, called hereafter activation probability, is the probability that neutron radiation induces radioactivity in material. Naturally, various isotopes are distributed non-uniformly throughout the body. This means that the concentration of a certain isotope in a specific organ may be higher than in others. Assuming the activation probability is invariable over the sample, photon emission from a part of the body will directly correspond to isotope abundance in that part. Thus, it is possible to estimate the amount of isotopes in the body, if uniform detection of induced photons is performed.

For the majority of isotopes, the probability of thermal neutron capture is higher than fast neutron capture. Therefore, fast neutrons have a negligible share of the activation process. Thereby, accurate measurement using IVNAA depends upon obtaining uniform thermal neutron flux (see uniformity section).

Nevertheless, because of low penetration depth of thermal neutrons, especially for large samples such as the human body, neutrons with higher energy (epithermal and fast) are required [5]. They lose their energy and fall into the thermal range as they penetrate into the different body

tissues. The feedback effect of a body on an external neutron field is a well-known phenomenon called self-shielding [6]. Therefore, thermal neutron flux and, consequently, activation rate in tissues depend on incident neutron spectrum and the anatomical characteristics of the body.

Incident spectrum depends on the types and the positions of neutron sources that are employed. The construction of the irradiation facility may also change the incident spectrum on the body surface. So the configuration of the system should be studied as well as neutron sources. Although, none of the irradiation facilities used for IVNAA is identical, decreasing the systematic error by increasing uniformity is an important aim in many of them. Various investigators have coped with this problem by optimizing the incident neutron spectrum. In 1967 Battye and his colleagues used a deuterium-tritium neutron (DT) generator to investigate thermal neutron flux profiles [7]. One year later, Chamberlain opted for a cyclotron (with a mean energy of approximately 3 MeV) as a neutron source to provide uniform distribution in a human cadaver [3]. In the same year, Palmer *et al.* compared a DT generator (14 MeV) and a cyclotron (average neutron energy was about 2 MeV) due to uniformity of activation probability in a large sample. They found that in order to get an approximately uniform flux throughout the thickness of the body, fast neutrons must be used [8].

The main basis for research in the 1970s was to design a facility that would increase the uniformity of thermal neutron flux in water phantoms [9, 10]. In order to improve the uniformity of depth distribution in the sample, the phantom was surrounded by hydrogenous material in all of this research. In 1973 Cohn *et al.* discussed the selection of neutron sources in total body neutron activation considering articles thitherto published [11]. According to this report, when bilateral irradiation is employed, the most uniform distribution is obtained with moderated 14 MeV neutrons. (α,n) sources such as ^{238}Pu-Be and ^{241}Am-Be produce a reasonably uniform distribution. This rather uniform distribution, coupled with the advantage gained through the use of a relatively low energy incident neutron (advantage factor = 2.1 relative to 14 MeV neutrons), renders the use of (α,n) sources attractive for total body neutron activation. An additional benefit accrues from the ease of operation and reproducibility inherent in constant-output radioactive neutron sources [11].

In the early 1980s, due to a lack of professional codes and advanced technology, research on this subject came to a halt for 10 years. The development of computers and calculation codes made simulation a strong instrument in nuclear medicine. Dr IE Stamatelatos is one of the researchers who used simulation to improve the IVNAA system. In 1992 and 1993 he presented results from a study comparing neutrons produced from (α,n) reactions and spontaneous fission sources on increasing uniformity. In addition, he amended the flux profile by simultaneously applying a reflector and pre-moderator [12, 13].

The Neutron Activation Research Centre (NARC) of Ferdowsi University of Mashhad tried to develop an IVNAA facility to study body composition at the Monash Medical Center [14]. This apparatus was designed to simultaneously measure total body nitrogen and chlorine in children. This work focuses on the measurement of total body chlorine in children.

In 2009 Miri *et al.* showed that thermal neutron flux and activation rate are higher for ^{252}Cf, however, (α,n) sources (specially ^{241}Am-Be) provide better uniformity. Four collimator materials (paraffin, borated paraffin, graphite and heavy water), two collimator shapes (pyramidal and rectangular) and two configurations (unilateral and bilateral) were investigated in the same work [5]. In addition, the effects of collimator aperture dimensions, presence or absence of the pre-moderator (PM) and reflector/moderator (R/M) and optimum thickness required to provide uniform distribution in a water phantom were surveyed in the next article [15]. The archetype used in the presented work is according to these studies. The other essential factor that should be considered is the human body. The size and shape of various regions of the human body cause thermal neutron flux to be dispensed non-uniformly. In addition, because of heterogeneities in the medium of different regions of the phantom, the thermal neutron flux profile may change and become non-uniform, even if the phantom has a simple symmetrical shape. Therefore, simulation using a more realistic body model rather than a water phantom is necessary.

Unfortunately, increasing the uniformity of thermal neutron flux will have a high cost. Using fast neutrons to improve uniformity, the dose delivered to the body increases [5, 16]. In addition, the activation of materials used in the facility may affect detector spectrum [17]. Thus, uniformity, absorbed dose and gamma spectrum should be inspected simultaneously.

In this work, in order to investigate activation rate distribution, we tried to improve the uniformity of thermal neutron flux in the 5-year-old stylized phantom described by Oak Ridge National Laboratory (ORNL) [18], by changing PMs and collimators. Different materials and thicknesses of PMs and collimators were examined. Finally, the facilities' properties such as uniformity parameters of thermal neutron flux distribution and the mean values of thermal neutron flux and activation rate distribution in the body, received dose to the patient, and the secondary photons contributing to the detected spectra were studied.

MATERIALS AND METHODS

The initial step in the study of PMs is the evaluation of the thermalizing capability of different materials. To assess the

appropriate choice of PM material, nine materials (water, paraffin, graphite, heavy water, borated paraffin, beryllium, aluminum, Teflon and Fluental) with three different thicknesses were investigated.

After determining PM material considering collimator as a neutron multiplier, six other facilities were studied too. In each part, uniformity indexes, mean values of thermal neutron flux and activation rate, and effective dose in the phantom as well as detected gamma rays were calculated using MCNPX code.

This section will first describe the facility, the changes made to the initial system and phantom characteristics in detail. Subsequent topics below highlight brief discussions about the main parameters used to compare different setups and Monte Carlo simulation details.

Facility description

The archetypal IVNAA facility was designed according to the Monash Medical Center's system in Australia [14]. The bilateral rectangular shape collimator contains graphite with four ^{241}Am-Be neutron sources, each containing 146.07 GBq (3.95 Ci). A concrete shield surrounds the collimator to protect the IVNAA operator. Two pairs of 10 cm × 10 cm × 15 cm NaI(Tl) detectors are positioned on both sides of the scanning bed, along a horizontal axis perpendicular to the vertical neutron beam. Each detector is shielded from neutrons by 2.5-cm-thick borated-paraffin housing. In addition, there are two lead sheets on the collimator to protect the detectors from undesirable gamma rays. To increase thermal neutron flux at the lateral surfaces, and to reduce neutron loses, R/M objects, which cover the sides of the phantom, were prepared. Figure 1 shows schematic views of the irradiation facility. In this setup, the bottom PM was considered as the patient bed. So, a solid container should be taken into account if the proposed PM is liquid (such as water and heavy water). The container was ignored in this work.

Pre-moderator

PM is a material inserted between the neutron source and the sample, in order to improve the thermal flux uniformity. Thermal neutron flux will not increase in the phantom unless the PM also has a high capability to moderate fast neutrons and small scattering angles. Due to the position of the PMs in the facility (the top and bottom of the phantom), PMs may increase thermal neutron flux in the surface layers of the body and smooth the depth distribution. Elastic scattering is a suitable way to decrease neutron energy. A good moderator is made of materials with low mass numbers. In addition, according to Equation 1, lighter materials have small scattering angles:

$$\overline{\cos\psi} \approx \frac{2}{3A} \quad (1)$$

Where ψ is the scattering angle of the neutron in the laboratory coordinate system, and A is atomic mass of the moderator [19]. As a result, hydrogenous materials such as water, paraffin and borated paraffin may be appropriate choices for moderating fast neutrons [8, 20]. With the capture of slow neutrons in hydrogen and inelastic scattering of carbon, 2.23 MeV and 4.43 MeV gamma rays are emitted, respectively. High photon production not only corrupts the detector spectra, but also may increase the delivered dose.

Figure 2A to D shows the macroscopic cross-sections of total, elastic, absorption and (n,2n) interactions of neutron with some compounds used in this paper [21]. It is clear that the elastic scattering cross-sections of water and paraffin (Fig. 2B) are greater than all mentioned materials except beryllium (Be). Such large cross-sections together with good thermalizing capability cause neutron energy to decrease.

After hydrogen, which is composed of a single proton, deuterium is the lightest nucleus. So heavy water should be a good moderator [22]. Moreover, neutron capture by deuterium produces a prompt gamma ray of 6.25 MeV, but with a cross-section less than hydrogen by a factor of about 640 [23]. Besides, heavy water has the smallest values of neutron absorption among all the other materials, so thermal neutrons can penetrate into it with negligible attenuation (Fig. 2C).

Graphite and Be are also light nuclei with great elastic scattering cross-sections (Fig. 2B) and comparatively small absorption cross-sections (Fig. 2C). On the other hand, Be has a high (n,2n) cross-section and can reduce neutron energy (Fig. 2D). So, these materials can be considered for PM.

Some other materials, which are usually used as moderators in Boron Neutron Capture Therapy (BNCT) facilities to provide epithermal neutron fluxes, are aluminum (Al), Fluental and polythetraflouroethylene (CF_2), commercially known as a Teflon [24, 25]. Fluental is a patented material with composition AlF_3 (69%), Al (30%) and LiF (1%) that was developed in Finland for reactor-based BNCT [26]. Hence, these PMs were also checked. As can be seen from Fig. 2, Fluental and Teflon have elastic scattering and total (which includes inelastic scattering) cross-sections presenting complementary resonances that allow the efficient reduction of the energy of fast neutrons. Moreover, Fig. 2A shows that the absorption cross-sections in the low energy range of Teflon are relatively low.

Except for Al, Fluental and Teflon, which are usually used with high thicknesses, other PMs were evaluated with three different thicknesses of 0.5 cm, 1.0 cm and 3.0 cm. For Al, Fluental and Teflon high thicknesses of 5.0 cm, 7.0 cm and 10.0 cm were studied.

Collimator

The collimator is a part of the system that steers neutron streams emitted from sources to the phantom. Enhancing

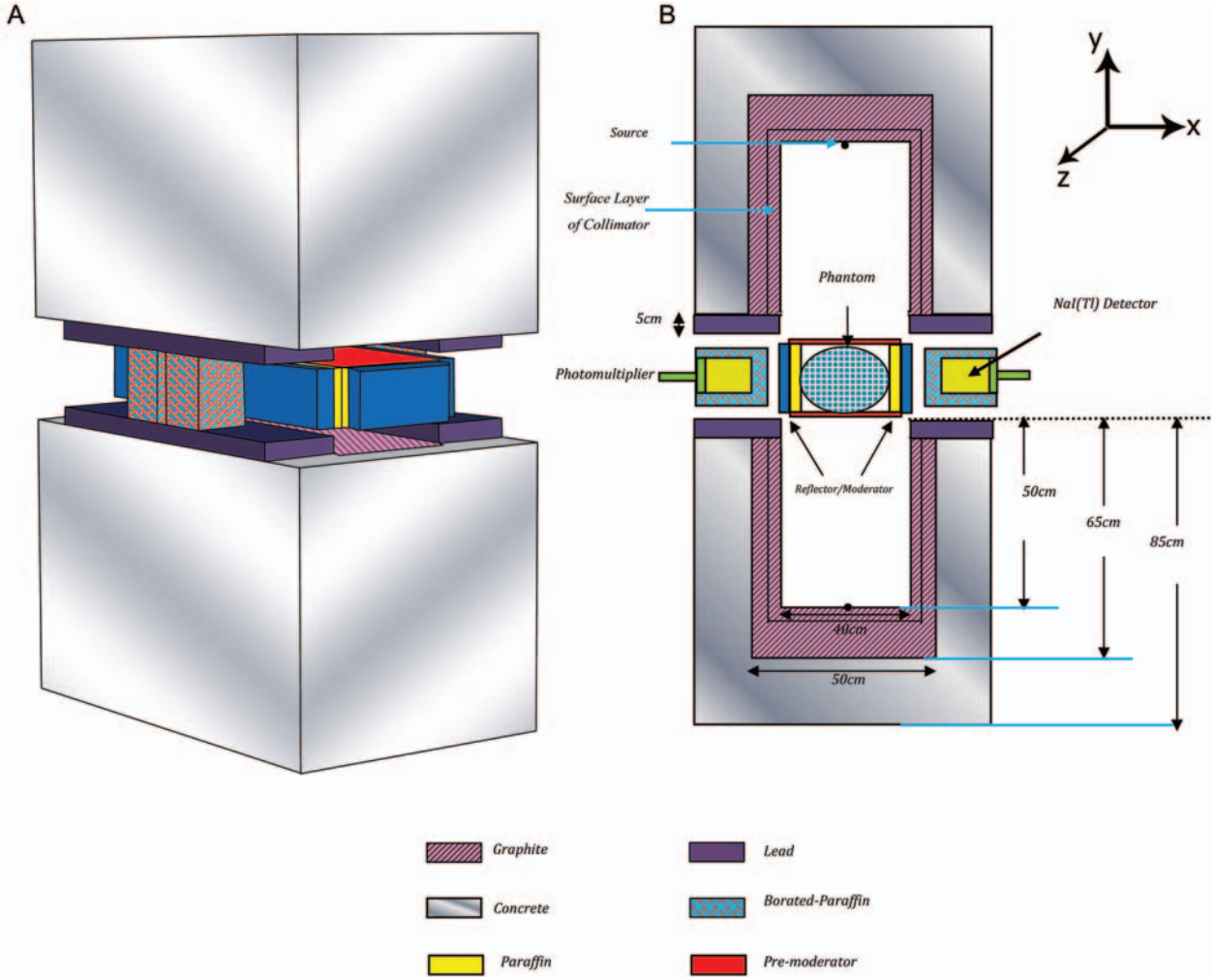

Fig. 1. Schematic view of the irradiation facility: (**A**) 3D-dimensional view; (**B**) a cross-sectional view. Only one pair of detectors and sources can be seen in this view.

neutron flux on the body, the collimator should be a good reflector. So, it should have a large scattering angle to prevent neutrons from escaping from the system. In consequence, based on equation 1, collimator material must have a large atomic mass. One goal of the present investigation was to use a collimator as a reflector and multiplier simultaneously to provide uniform distribution of thermal neutron flux.

For this purpose, a surface layer of the collimator was replaced with materials with a large atomic mass and high (n,2n) cross-section such as beryllium (Be), lead (Pb) and bismuth (Bi) (see Fig. 2D). Results were compared with the initial facility in the following section.

Characteristics of the phantom

A mathematical/numerical phantom is a mathematical representation of the human body and includes all relevant information. All organs are represented with analytical geometry bodies (e.g. cylinders, ellipsoids, cones), which are described with suitable mathematical equations. The corresponding chemical composition of various types of organ tissues is also defined.

The generation of the anatomical phantoms originated at Oak Ridge National Laboratory (ORNL). Until now researchers have introduced several revised versions of these models [27, 28]. In this study, we modified the ORNL 5-year-old phantom, which concludes the revisions reported by Han *et al.* in 2006, and the thyroid model provided by Ulanovsky was simulated with MCNPX [29, 30].

This phantom has a length of 110 cm, width of 30 cm and a depth of 16 cm. The geometry of the sample was constructed with four major parts: (i) an elliptical cylinder representing the trunk and arm; (ii) a half ellipsoid placed on top of an elliptical cylinder as a head; (iii) another elliptical cylinder between the head and trunk representing the neck; and (iv) two truncated circular cones

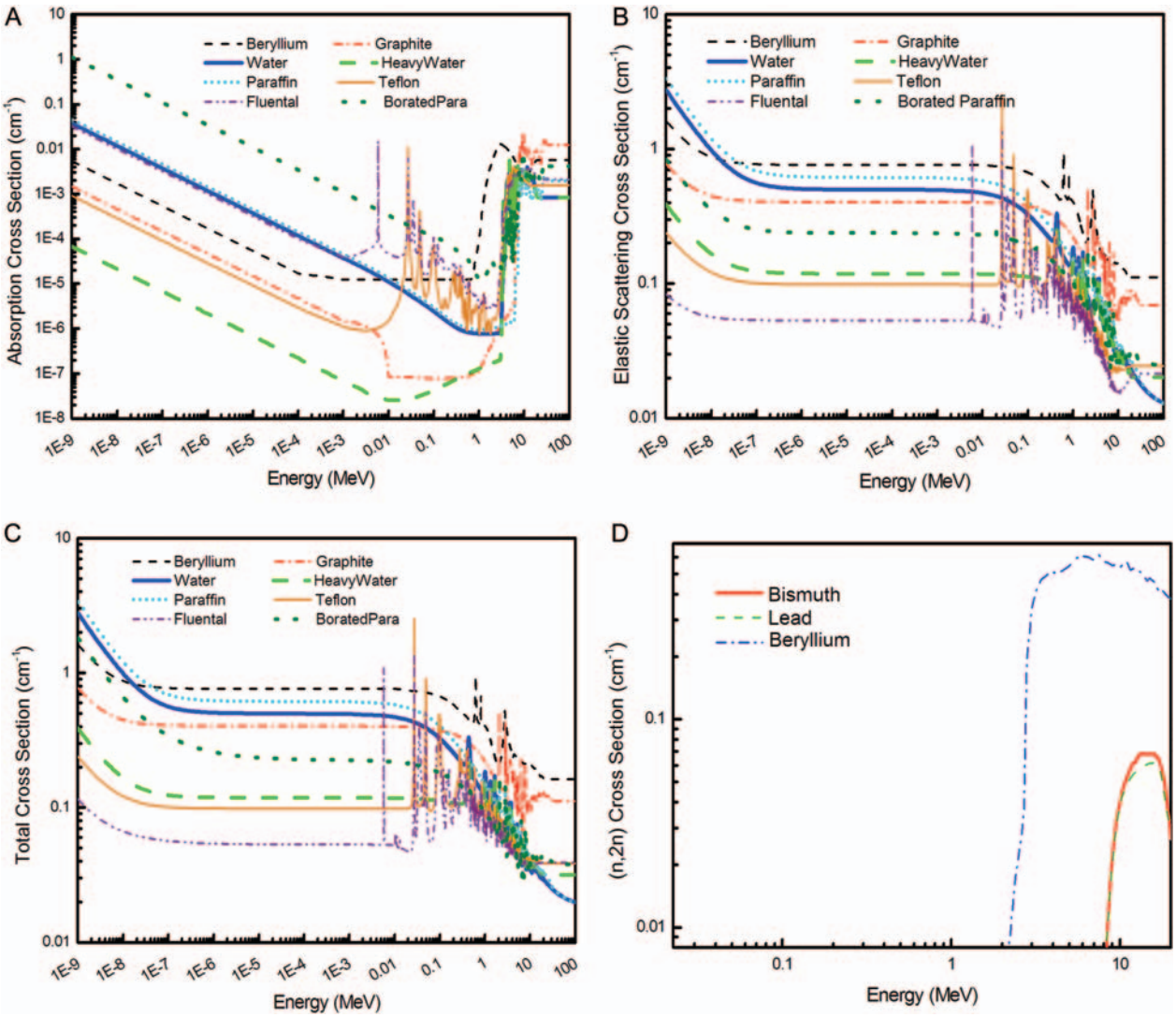

Fig. 2. Macroscopic cross-section of neutron interactions with some compounds used in this paper: (**A**) absorption; (**B**) elastic scattering; (**C**) total; (**D**) (n,2n).

that represent the legs and feet [17]. The elemental composition and density of three major body tissues (skeletal, lung and soft tissue) were chosen from Table A-1 of ORNL/TM8381 [27].

Uniformity

A basic problem with IVNAA technique is obtaining uniformity of activation rate distributions in the body. As aforementioned, the spectrum of gamma rays, which emerge immediately after activation, is analyzed to determine the amount of the quantity of some isotopes. Thus, more emitted photons from a certain organ than from others implies a higher concentration of isotope in that organ. An accurate measurement requires ideally that activation probability is the same for all atoms of a specific isotope, irrespective of location in the body or of the body shape. Since thermal absorption cross-section is much higher than fast absorption cross-section for the majority of the nuclei, one can ignore the contribution of the fast neutrons to the activation rate. Hence the relationship between activation rate density (A) and thermal neutron flux (ϕ) is as follows [31]:

$$A \approx N\sigma_{\mathrm{th}}\varphi_{\mathrm{th}} \tag{2}$$

Where N is the number of nuclei per unit volume and σ_{th} is the microscopic cross section for thermal neutrons. As can be observed, if the activation probability, which is equal to the product of the microscopic cross-section and neutron flux, is constant; activation rate density will be proportional to N.

Generally, the coefficient of variation (CV) is used to evaluate the uniformity of thermal neutron distribution. CV looks at the variability of data points and estimates the deviation of data from the mean value:

$$CV = \frac{\sigma_x}{\bar{x}} \tag{3}$$

Where σ_x and $\bar{x}$ are the standard deviation and mean, respectively. The CV value, as is often with such reports, is expressed in percent. The aim of this work is reduction of CV value to around 10%, by designing an appropriate combination of PM and collimator in the facility. Another parameter that could be useful to study the data dispersion is Maximum to Minimum Ratio (MMR). This parameter is also reported in this paper.

Additional useful instruments to study uniformity are Cumulative Volume Histograms (CVH) of thermal neutron flux and activation rate. The purpose of a CVH is to summarize some 3D distributions in a graphical 2D format. By way of illustration, the CVH of the activation rate is plotted with bin activation rates along the horizontal axis and the column height of each bin represents the volume fraction (in percent) of structure activating with greater than or equal to that rate. With very fine bin sizes, the CVH of the activation rate takes on the appearance of a smooth line graph. The lines always slope and start from top-left to bottom-right. If the activation rate is distributed homogenously the CVH of the activation rate will appear as a horizontal line at the top of the graph [32, 33].

Dosimetry

Effective dose provides an approximate indicator of potential detriment from ionizing radiation. In accordance with ICRP publication 103, effective dose (E) is obtained by the following equation [34]:

$$E = \sum_T w_T \sum_R w_T D_{T,R} \tag{4}$$

Where $D_{T,R}$ (organ absorbed dose) is the quotient of deposited energy due to radiation of type R in the volume of a specific organ or tissue T by its mass. The SI unit of organ absorbed dose is J kg^{-1}, and the special name for the unit is the gray (Gy). Effective dose is often expressed in sievert (Sv), so that 1 Sv = 1 J kg^{-1}.

Also, w_R and w_T are the appropriate radiation weighting factor and tissue weighting factor, respectively [34]. In order to determine the radiation weighting factors with high accuracy, it is essential to specify the exact energy of incident neutrons on the body. In an IVNAA facility, however, the incident energy spectrum of neutrons on the body will be difficult and time consuming to specify, because of the changes in the incident neutron energy spectrum in the presence of the collimators, moderators and reflectors. There is another method that can estimate effective dose with an acceptable approximation (Araghian N, Rafat Motavalli L, Miri Hakimabad H. Optimization of the BCA facility using the γ shield and improvement of accuracy using ORNL anthropomorphic phantoms (To be submitted), http://profsite.um.ac.ir/~mirihakim/14th%20IVNAA%20Project.pdf). The effective dose can be ascertained using the organ dose equivalent ($\overline{H}_T$):

$$\overline{H}_T \approx \sum_R Q_R D_{T,R} \tag{5}$$

$$E \approx \sum_T w_T \overline{H}_T \tag{6}$$

Where Q_R is the quality factor for particles as a function of energy at the tissue location of interest [34]. This was examined in real systems such as the IVNAA facility in a comprehensive study in NARC and has been verified (Araghian N, Rafat Motavalli L, Miri Hakimabad H. Optimization of the BCA facility using the γ shield and improvement of accuracy using ORNL anthropomorphic phantoms (To be submitted), http://profsite.um.ac.ir/~mirihakim/14th%20IVNAA%20Project.pdf).

In this study, the neutron quality factors were chosen from the NCRP 38 report [35]. Figure 3 shows the neutron quality factors that were reported in NCRP 38. Since the quality factors for photons are equal to one at any energy level, the organ absorbed doses due to photons and their organ dose equivalents are the same. Furthermore, the tissue weighting factors were selected from the ICRP 103 report [34].

For two setups that are somewhat similar in terms of uniformity, setups with lower effective dose and higher mean value are preferred. To compare such situations, the ratio of thermal neutron flux to effective dose, which is known as

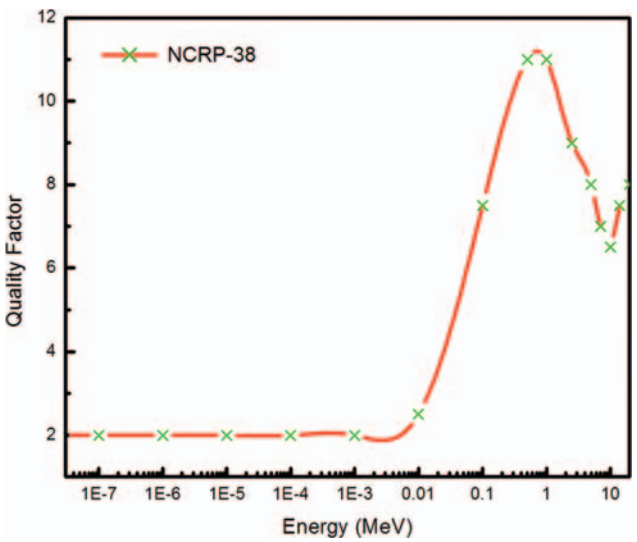

Fig. 3. Neutron quality factors versus energy, which were previously reported in NCRP 38.

sensitivity, should be calculated. It is clear that the greater sensitivity means a lower effective dose is received by the patient during irradiations for IVNAA.

Secondary photons

In an IVNAA system, in addition to the sample, other parts of the facility are also exposed to the neutron sources and so, may be activated. Some of the produced photons in these parts travel a relatively short distance, whereas others pass through or penetrate the facility. Thus, detectors may confront gamma rays not only from the sample, but also from other parts of the setup, which may corrupt the spectrum. In order to have a reliable detection, an ideal spectrum should be extracted from the final detector spectrum. The ideal situation is a situation in which all gamma rays that reach the detector are solely from the sample, omitting all of the gamma rays that are produced in other parts of the system. This situation can be simulated when photon production is turned on only in the phantom. The evaluated spectrum can be analyzed and calibrated to measure the precise amount of sample elements [17]. If the energy of the secondary photons that were produced inside the different components of the facility lie in the region of interest (ROI), distinguishing the ideal peak will be difficult. This paper focuses on chlorine, the ROI in the spectrum data is between about 5.5 MeV and 8.00 MeV [23].

To investigate the effect of the proposed PM and/or collimator on the detected spectrum, study of the photons that reach the detector from these parts is necessary. For this purpose, photon production was turned on in just the phantom and PM and/or collimator and obtained spectra were compared with the ideal situation. It is essential to note that detector spectra obtained under these conditions are not the real ones, because the photons produced in other parts of facility were ignored.

Monte Carlo simulations

The basis of the design studies were neutron transport calculations performed using the Monte Carlo N-Particle code, MCNPX 2.4.0. MCNPX is a general purpose Monte Carlo radiation transport code for modeling the interaction of radiation with materials [36]. The verification of the models was approved by comparing the results with experimental ones in previous work [5]. The cross-sections used in this study were chosen from the ENDF/B-VI libraries [21]. Molecular effects and scattering treatment, S(α,β), were considered for neutrons below 4 keV (MTm card) in all calculations that included neutron transport. The neutron energy spectrum was simulated, according to the report by Kluge *et al.* published in 1982 [37], and gamma rays of ^{241}Am-Be were chosen based on a previous study by Miri *et al.* [38].

To analyze volumetric distributions and evaluate their uniformity index, it is necessary to divide the phantom into adequately small volume elements and determine thermal neutron flux and activation rate in each of them. Nevertheless, miniaturizing volume elements is restricted because if cell dimensions are very small, the numbers of statistical errors in the reasonable time would be large. Thus, the phantom was partitioned by a 3D rectangular mesh grid into about 23 000 volume elements of 1 cm × 1 cm × 1 cm. Neutron flux values were calculated using track averaged mesh tallies (keyword: flux) and activation rates were determined using the same mesh tallies together with the appropriate FM card. Then neutron flux in the range of thermal energies ($E < 5 \times 10^{-7}$ MeV) was also scored in meshes. The statistical uncertainties of thermal neutron flux and activation rate were around 2.5% and running time lasts over 6 days.

Since IVNAA is used with humans, dose calculation is very important. Therefore, energy deposition in separate organs (organ absorbed dose) and effective dose for the whole body were computed. To estimate absorbed dose in each organ, track length estimation of energy deposition (F6) was employed. Also, the organ dose equivalent was obtained by the product of the absorbed dose in quality factors using DE and DF cards. Neutron and neutron-induced photon doses due to the neutron source as well as the photon dose due to the photons directly emitted from the source were calculated separately. It should be noted that for the ^{241}Am-Be source, the ratio of photons per neutron emission is 0.591 [39]. Thus, the values obtained from the photon source must be multiplied by this correction factor.

To study the effect of secondary photons produced in the region investigated on an ideal spectrum, it is necessary to run other MCNP simulations. In these programs, a PWT card was applied and track length tally (F4) was utilized to determine photon flux in the detectors. The PWT card is used to control the number and weight of neutron-induced photons produced by neutron collisions [40]. Analyzing the effect of changing the type and thickness of the PM and/or collimator on ideal spectrum, secondary photon production was turned off all over the system except in the phantom and these parts of the facility. Detector spectra were compared for photon energies lower than 7 MeV with statistical error of the order of about 5%, in most cases even less. To consider detector resolution, the initial responses of the MCNP calculation were broadened with a FT card together with the GEB (Gaussian Energy Broadening) option using appropriate indices of the experimentally applied detector [38].

All calculated values were normalized by number of neutrons emitted (in 4π steradians) by ^{241}Am-Be sources during a time interval of 1 min. To do this, the values of the simulated data presented in this work were multiplied by factor of about 2×10^{9} (min^{-1}), which is equal to the product of: 4 (source number) $\times 5.9 \times 10^{-5}$ $(Bq.s)^{-1}$

(neutron yield per decay) × 146.07 GBq (source activity) × 60 (s.min^{-1}).

RESULTS

Results were classified into three categories: (i) pre-moderator; (ii) collimator; and (iii) final setup. The 'pre-moderator' section focuses on the effect of the type and thickness of PM on the activation rate distribution inside the phantom. Uniformity and dosimetry parameters were computed for several setups that were different in terms of type and thickness of PM. After selection of PM material, a surface layer of the collimator was replaced with materials that are good neutron multipliers. In the second section, the type and thickness of the multiplier layer and the thickness of the PM were changed simultaneously. After comparing main parameters (uniformity, dosimetry and detector spectrum), a final facility was proposed.

Pre-moderator

Table 1 lists the CV percentage, MMR and mean values of thermal neutron flux for different PM materials. To estimate the quantity of elements, the activation rate values are needed. These values, which were obtained by multiplying activation rate density by volume element (1 cm^3), are presented in Table 2. Attending to dosimetry considerations, effective dose and sensitivity are also provided in this table. Three thicknesses were evaluated to simplify the initial estimation. The statistical errors of mean value and effective dose are about 0.01% and 0.5%, respectively.

Al, Fluental and Teflon are typically used with high thicknesses for moderating. The results obtained with high thicknesses of these materials are presented in Tables 3 and 4. In order to compare the different materials in terms of neutron-induced photon production, detector spectra in different situations are indicated in Fig. 4. These spectra belong to the facilities, which are similar in terms of thickness of PM (1.0 cm) but with different types of PM.

As is evident from Tables 1–4, hydrogenous materials such as paraffin and water provide better uniformity than other materials. Although the CV percentage, mean value and effective dose of paraffin and water PMs are somewhat similar, the sensitivity of paraffin is greater. According to Fig. 4B, secondary photon spectra of the facilities with water and paraffin PMs are also similar in the chlorine region of interest. For this work, paraffin was selected as the PM type.

Collimator

In this section, the surface layer of the graphite collimator was replaced with some materials with a high (n,2n) cross-section. With regard to the results in the previous section, two paraffin slabs in the top and bottom of the phantom were used as PMs. To achieve the optimal situation, different thicknesses of PM were studied.

Required parameters to investigate the priority of different situations, in terms of uniformity, mean values of thermal neutron flux and activation rate and dosimetry are indicated in Tables 5 to 7, respectively. As can be seen, CV values and effective doses as well as the mean values of activation rate decrease with increasing PM thickness. It can be seen that with a high thickness of paraffin (10 cm), the CV value becomes close to around 10%. However, because of the secondary photon problem that will be discussed later (see Discussion section), PM thickness is restricted to about 3 cm in the present study. For thicknesses of less than 3 cm, the Be collimator has the smallest CV values. But the detected spectrum with a Be collimator

Table 1. Uniformity indexes and mean value of thermal neutron flux with different types and thicknesses of PM

PM type	CV%			MMR			Mean value of thermal neutron flux (×10^5 min^{-1})		
	0.5 cm	1.0 cm	3.0 cm	0.5 cm	1.0 cm	3.0 cm	0.5 cm	1.0 cm	3.0 cm
Paraffin	15.6	13.9	12.6	2.6	2.6	2.6	1.97	2.03	1.89
Graphite	19.0	18.0	15.9	2.7	2.6	2.5	1.80	1.8	1.76
Heavy water	18.7	17.5	14.9	2.6	2.6	2.5	1.80	1.82	1.83
Water	16.2	14.3	12.6	2.6	2.5	2.5	1.94	2.00	1.94
Borated-paraffin	20.8	21.01	18.9	3.3	3.6	3.6	1.66	1.51	1.11
Beryllium	18.3	17.0	14.7	2.6	2.5	2.6	1.83	1.84	1.85
Aluminum	20.0	19.7	19.5	2.7	2.7	2.8	1.77	1.74	1.64
Fluental	20.3	20.4	22.0	2.8	2.9	3.3	1.73	1.66	1.47
Teflon	19.0	18.0	15.9	2.6	2.5	2.4	1.78	1.77	1.72
Without		20.2			2.7			1.79	

Table 2. Mean value of activation rate and dosimetry parameters with different types and thicknesses of PM

PM type	Mean value of activation rate ($\times 10^3$ min^{-1})			Effective dose (μSv.min^{-1})			Sensitivity ($\times 10^4$ μSv^{-1})		
	0.5 cm	1.0 cm	3.0 cm	0.5 cm	1.0 cm	3.0 cm	0.5 cm	1.0 cm	3.0 cm
Paraffin	4.14	4.28	4.01	19.1	17.6	12.9	1.03	1.15	1.47
Graphite	3.76	3.76	3.70	20.0	19.6	16.9	0.90	0.92	1.04
Heavy water	3.81	3.83	3.87	19.5	18.5	14.8	0.92	0.98	1.24
Water	4.10	4.24	4.12	19.4	18.1	14.1	1.00	1.11	1.38
Borated-paraffin	3.45	3.16	3.45	19.1	17.6	13.0	0.87	0.86	0.85
Beryllium	3.83	3.87	3.91	19.6	18.5	14.8	0.93	1.00	1.25
Aluminum	3.70	3.64	3.45	20.1	19.5	17.6	0.88	0.89	0.93
Fluental	3.62	3.47	3.06	19.9	19.0	16.0	0.87	0.87	0.92
Teflon	3.74	3.72	3.62	19.9	19.1	16.3	0.89	0.93	1.06
Without		3.76			20.63			0.87	

Table 3. Uniformity indexes and mean value of thermal neutron flux with aluminum, Fluental and Teflon used as PMs with high thicknesses

PM type	CV%			MMR			Mean value of thermal neutron flux ($\times 10^5$ min^{-1})		
	5 cm	7 cm	10 cm	5 cm	7 cm	10 cm	5 cm	7 cm	10 cm
Aluminum	19.4	19.4	19.4	2.9	2.9	3.0	1.57	1.50	1.73
Fluental	22.0	22.4	22.6	3.4	3.6	3.4	1.32	1.20	1.07
Teflon	14.9	14.4	13.9	2.5	2.6	2.5	1.66	1.60	1.51

Table 4. Mean value of activation rate and dosimetry parameters with aluminum, Fluental and Teflon used as PMs with high thicknesses

PM type	Mean value of activation rate ($\times 10^3$ min^{-1})			Effective dose (μSv.min^{-1})			Sensitivity ($\times 10^4$ μSv^{-1})		
	5 cm	7 cm	10 cm	5 cm	7 cm	10 cm	5 cm	7 cm	10 cm
Aluminum	3.29	3.12	2.94	15.6	13.9	11.9	1.01	1.08	1.45
Fluental	2.75	2.50	2.23	13.6	11.4	8.9	0.97	1.05	1.20
Teflon	3.50	3.37	3.19	13.8	11.9	9.4	1.20	1.34	1.61

differs greatly from the ideal spectrum in the chlorine region (Fig. 5). Looking at the other elements, a Pb layer did not give a reasonable CV value and effective dose. A graphite collimator and graphite collimator with 2 cm Bi had similar results but the mean value and sensitivity of the latter were slightly higher. Also the detector spectrum of the collimator with a Bi layer matched better with the ideal spectrum. It seems that replacing the surface layer of the collimator with 2 cm Bi and using 3 cm paraffin improves the main parameters of the IVNAA facility.

Final facility

This section takes into consideration some of the characteristics of the final facility. CVH graphs of activation rate and thermal neutron flux for the whole body and some of the important organs are presented in Fig. 6. Figure 7

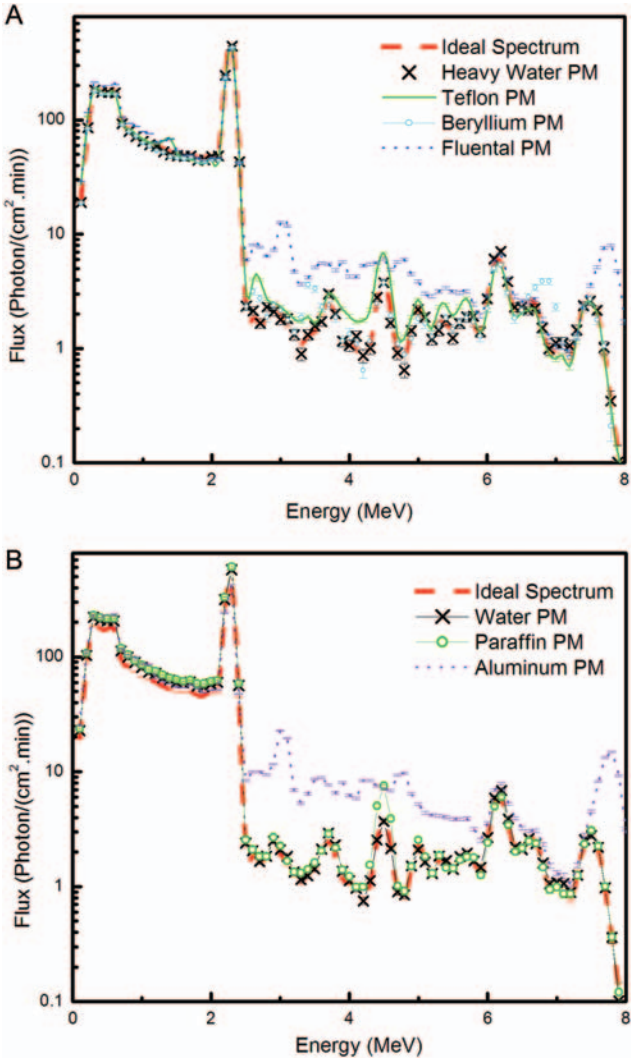

Fig. 4. Detector spectrum using different PMs with similar thicknesses (1.0 cm).

illustrates a 2D plot of the activation rate, thermal neutron flux, fast neutron flux and energy deposition in a two-dimensional array at mid-depth of the phantom using a mesh tally of MCNPX code. The phantom was placed in a rectangular grid composed of 70 400 unit volume elements, of which just 23 000 elements were within the phantom. Thus, activation rate, flux and energy deposition were only reported through the phantom and the values of these parameters were considered to be zero outside the body.

DISCUSSION

Pre-moderator

If the neutron sources merely have a thermal range, because of the high absorption capacity of matter for thermal neutrons, the activation rate falls off rapidly with depth within the body. So, using sources that emit high-energy neutrons is unavoidable. When such high-energy neutrons pass through the surface layers of the body, they lose their energy and are slowed down, by elastic or inelastic scattering reactions with their surroundings. Therefore, thermal neutron flux increases at the mid-depth of the phantom. In the absence of PM, thermal neutron flux distribution is raised in the middle part of the body, in contrast with the two ends. PM causes fast/epithermal neutrons to lose their energy and fall to epithermal/thermal range before they arrive at the body surface. In other words, the important role of the PM is to smooth depth activation. In addition, it is possible that some of the thermal neutrons, arriving directly from the sources, are absorbed into the PM. So the mean value of activation rate may decrease in the body. It is worth mentioning that because the activation rate is also dependent on the number of nuclei per unit volume, the CV value of the activation rate would be higher than that for the thermal neutron flux.

As is evident from Tables 1 and 3, the CV values of the Al and Fluental PMs are around the same as in a setup without a PM; with high thicknesses of Fluental the CV value is even higher. Other PMs, except borated paraffin, provide a fairly satisfactory uniform distribution in the body. Hence, a comparison should be done between the other parameters, advantages and disadvantages of these PMs.

As shown in Fig. 4, with Al, Fluental and Teflon PMs, gamma ray spectra are dominated by peaks from the PM material and differ greatly from the ideal situation. Figure 8 illustrates the prompt gamma neutron activation cross-section in terms of photon energy of Al and fluorine [22]. It can be observed that Al and fluorine have a high number of peaks in the range of 0–8 MeV. Thus, Al, Fluental and Teflon are omitted not only because of their high CV values, but also due to the production of undesired background noise in the detector spectrum.

Regarding Table 1, it is expected that by increasing the thickness of Be, the CV value can be reduced. Although Be is a light element, the high ability of (n,2n) causes increasing epithermal neutron flux on the surface of body. On the other hand, because of momentum conservation, at least one of the neutrons produced in this reaction is directed toward the phantom. Nevertheless due to its spectrum, which has a peak at energies between 6 MeV and 7 MeV in chlorine ROI, it is not a good option to be used as a PM.

Among the other materials, paraffin and water have favorable uniform distributions with higher mean values than heavy water and graphite. In fact, hydrogen and neutrons have approximately identical masses. Thus, a neutron loses maximum energy in collision with a hydrogen atom. On the other hand, the small scattering angle of hydrogen makes hydrogenous material very convenient for the

Table 5. Uniformity indexes of thermal neutron flux with various thicknesses of paraffin PM and different collimators

Collimator layer	Graphite collimator Graphite		2.0 cm beryllium		5.0 cm beryllium		2.0 cm lead		5.0 cm lead		2.0 cm bismuth		5.0 cm bismuth	
Paraffin thickness (cm)	**% CV**	**MMR**	**% CV**	**MMR**	**% CV**	**MMR**	**% CV**	**MMR**	**% CV**	**MMR**	**% CV**	**MMR**	**% CV**	**MMR**
Without PM	20.2	2.7	17.0	2.4	13.7	2.4	22.8	3.1	25.9	3.6	21.5	2.9	23.5	3.1
0.5	15.6	2.6	13.4	2.4	11.7	2.2	16.9	2.8	18.7	3.2	16.3	2.7	17.5	2.9
1.0	13.9	2.6	12.4	2.5	11.5	2.1	14.7	2.8	15.8	3.0	14.2	2.7	15.1	2.7
1.5	13.1	2.6	12.2	2.3	11.8	2.1	13.6	2.7	14.4	3.0	13.2	2.7	13.9	2.8
2.0	12.7	2.6	12.3	2.4	12.2	2.1	13.1	2.7	13.6	2.9	12.9	2.6	13.2	2.7
2.5	12.6	2.6	12.5	2.3	12.7	2.0	12.9	2.6	13.3	2.9	12.8	2.7	13.2	2.7
3.0	12.6	2.5	12.7	2.3	13.0	1.9	12.9	2.6	13.3	2.9	12.7	2.5	12.9	2.7
3.5	12.7	2.5	13.0	2.3	13.3	1.9	13.0	2.6	13.2	2.8	12.7	2.5	12.9	2.7
4.0	12.6	2.4	13.0	2.3	13.4	1.9	12.9	2.6	13.2	2.8	12.6	2.4	12.9	2.6
4.5	12.6	2.4	13.0	2.2	13.4	1.9	12.9	2.4	13.1	2.7	12.8	2.5	12.9	2.5
5.0	12.5	2.3	12.9	2.2	13.3	1.9	12.8	2.5	13.1	2.6	12.6	2.3	12.9	2.6
6	12.3	2.1	12.5	2.0	13.1	1.9	12.6	2.3	12.9	2.5	12.4	2.2	12.7	2.4
8	11.4	2.0	12.0	2.0	12.9	2.0	11.9	2.1	12.1	2.2	11.6	2.0	11.9	2.2
10	10.7	1.8	12.0	2.0	13.9	2.4	11.1	1.9	11.1	1.9	10.9	1.8	11.2	1.8

forward moderator. Therefore, hydrogenous materials such as water and paraffin would be appropriate choices.

Figure 5 compares the induced activities resulting from irradiation of the phantom and the PMs. It is evident that the gamma spectrum for a water PM has a good agreement with the ideal spectrum as well as does the spectrum for a paraffin PM. The difference between the spectra obtained when water and paraffin are PMs is presumably due to the gamma rays generated via the inelastic scattering of neutrons with the carbon nucleus (4.43 MeV) in paraffin. However, both of these PMs are suitable considering the chlorine ROI.

Another limiting factor in IVNAA is the dose absorbed during the procedure. Clearly, it is desirable to deliver the smallest dose possible with the highest activation. The sensitivity analysis allows one to specify the setup that has the smallest effective dose with a reasonable mean value of activation. A paraffin PM is superior to water and heavy water PMs in terms of sensitivity. Moreover, using liquid PMs has some problems such as the necessity to waterproof containers, and the difficulty in transporting them, if there is a need to move the bed. For the aforementioned reasons, paraffin was selected as the PM material.

Collimator

Using a neutron multiplier collimator can compensate for thermal neutron flux reduction and enhance the uniformity in the sample. As can be seen in Tables 5–7, although a higher thickness of PM increases the moderation capability and the uniformity of thermal neutron flux, a greater number of thermal neutrons are absorbed into the PM, reducing the mean value of the activation rate. As a result of the flux reduction, the production of characteristic photons is reduced in the phantom and thus statistical error grows in the detector. Under these conditions, to obtain a reasonable result, the exposure time with a particular source should be increased. Moreover, because this enhances the production of undesirable photons in the PM (4.43 and 2.23 MeV), it is likely that the patient will receive a higher gamma dose. Table 8 shows that total effective dose was reduced by increasing the thickness of PM material. It could be the effect of the decreasing fast neutron population in the phantom and neutron dose decrement.

Studying the outcomes of Tables 5–8 indicates that despite reducing CV, MMR and effective dose in a setup with a thick PM, the reduced activation rate within the body makes it difficult to decide whether or not a thick PM is appropriate to use. Under these conditions, sensitivity could be an instrumental parameter. In accordance with the results, thicker paraffin slabs improve the sensitivity of the facility. However, there still remains the essential argument of whether or not the high photon production in thick PM corrupts the detector spectrum. Although the photons

Table 6. Mean values of thermal neutron flux ($\times 10^5$ min^{-1}) and activation rate ($\times 10^3$ min^{-1}) with various thicknesses of paraffin PM and different collimators

Collimator layer	Graphite collimator		2.0 cm beryllium		5.0 cm beryllium		2.0 cm lead		5.0 cm lead		2.0 cm bismuth		5.0 cm bismuth	
Paraffin thickness (cm)	**Thermal flux**	**Activation rate**	**Thermal flux**	**Activation rate**	**Thermal flux**	**Activation rate**	**Thermal flux**	**Activation rate**	**Thermal flux**	**Activation rate**	**Thermal flux**	**Activation rate**	**Thermal flux**	**Activation rate**
Without PM	1.79	3.96	2.52	5.29	3.16	6.64	1.81	3.79	1.74	3.64	1.81	3.79	1.74	3.64
0.5	1.97	4.14	2.71	5.71	3.31	6.99	2.01	4.24	1.98	4.18	2.00	4.22	1.94	4.10
1.0	2.03	4.28	2.74	5.79	3.29	6.97	2.10	4.43	2.09	4.41	2.07	4.38	2.03	4.30
1.5	2.04	4.32	2.70	5.73	3.20	6.78	2.12	4.47	2.13	4.49	2.09	4.43	2.06	4.36
2.0	2.00	4.26	2.62	5.56	3.06	6.52	2.10	4.45	2.12	4.49	2.07	4.38	2.04	4.32
2.5	1.96	4.16	2.52	5.36	2.90	6.16	2.05	4.34	2.08	4.41	2.02	4.28	2.00	4.24
3.0	1.89	4.01	2.39	5.09	2.73	5.81	1.98	4.20	2.01	4.26	1.95	4.14	1.94	4.14
3.5	1.81	3.85	2.26	4.82	2.55	5.44	1.90	4.03	1.93	4.12	1.87	3.97	1.87	3.97
4.0	1.73	3.68	2.13	4.53	2.38	5.09	1.81	3.85	1.84	3.93	1.78	3.79	1.78	3.79
4.5	1.64	3.50	1.99	4.24	2.21	4.72	1.71	3.64	1.76	3.72	1.69	3.60	1.69	3.60
5.0	1.56	3.31	1.86	3.97	2.06	4.38	1.62	3.45	1.66	3.54	1.60	3.39	1.60	3.41
6	1.39	2.96	1.62	3.47	1.77	3.79	1.44	3.08	1.48	3.14	1.42	3.04	1.43	3.04
8	1.10	2.34	1.24	2.65	1.34	2.85	1.13	2.42	1.16	2.48	1.12	2.38	1.13	2.40
10	0.88	1.86	0.97	2.09	1.04	1.08	0.90	1.92	0.92	1.96	0.89	1.90	0.89	1.90

Table 7. Effective dose and sensitivity of the setups with various thicknesses of paraffin PM and different collimators

Collimator layer	Graphite collimator		2.0 cm beryllium		5.0 cm beryllium		2.0 cm lead		5.0 cm lead		2.0 cm bismuth		5.0 cm bismuth	
Paraffin thickness (cm)	Effective dose (μSv. min^{-1})	Sensitivity ($\times 10^4$ μSv^{-1})	Effective dose (μSv. min^{-1})	Sensitivity ($\times 10^4$ μSv^{-1})	Effective dose (μSv. min^{-1})	Sensitivity ($\times 10^4$ μSv^{-1})	Effective dose (μSv. min^{-1})	Sensitivity ($\times 10^4$ μSv^{-1})	Effective Dose (μSv. min^{-1})	Sensitivity ($\times 10^4$ μSv^{-1})	Effective dose (μSv. min^{-1})	Sensitivity ($\times 10^4$ μSv^{-1})	Effective dose (μSv. min^{-1})	Sensitivity ($\times 10^4$ μSv^{-1})
Without PM	20.6	0.87	19.9	1.27	19.3	1.64	20.8	0.87	21.3	0.82	20.3	0.89	20.4	0.85
0.5	19.1	1.03	18.3	1.48	17.7	1.87	19.1	1.05	19.4	1.02	18.7	1.07	18.6	1.04
1.0	17.6	1.15	16.9	1.62	16.3	2.02	17.5	1.20	17.8	1.17	17.2	1.20	17.1	1.19
1.5	16.3	1.25	15.6	1.73	15.1	2.12	16.1	1.32	16.3	1.31	15.9	1.31	15.8	1.30
2.0	15.1	1.32	14.4	1.82	13.9	2.20	14.9	1.41	15.1	1.40	14.6	1.42	14.4	1.42
2.5	14	1.40	13.3	1.89	12.9	2.25	13.8	1.49	13.9	1.50	13.6	1.49	13.3	1.50
3.0	12.9	1.47	12.4	1.93	12	2.28	12.8	1.55	12.8	1.57	12.6	1.55	12.3	1.58
3.5	12	1.51	11.5	1.97	11.1	2.30	11.8	1.61	11.9	1.62	11.6	1.61	11.4	1.64
4.0	11.2	1.54	10.7	1.99	10.3	2.31	10.9	1.66	11	1.67	10.8	1.65	10.6	1.68
4.5	10.4	1.58	9.9	2.01	9.6	2.30	10.2	1.68	10.2	1.73	10.1	1.67	9.9	1.71
5.0	9.8	1.59	9.3	2.00	9	2.29	9.5	1.71	9.5	1.75	9.4	1.70	9.3	1.72
6	8.6	1.62	8.1	2.00	7.8	2.27	8.4	1.71	8.3	1.78	8.2	1.73	8.1	1.77
8	6.6	1.67	6.3	1.97	6.1	2.20	6.4	1.77	6.3	1.84	6.3	1.78	6.3	1.79
10	5.2	1.69	5.1	1.90	4.8	2.17	5.1	1.76	5.0	1.84	5.1	1.75	5.0	1.78

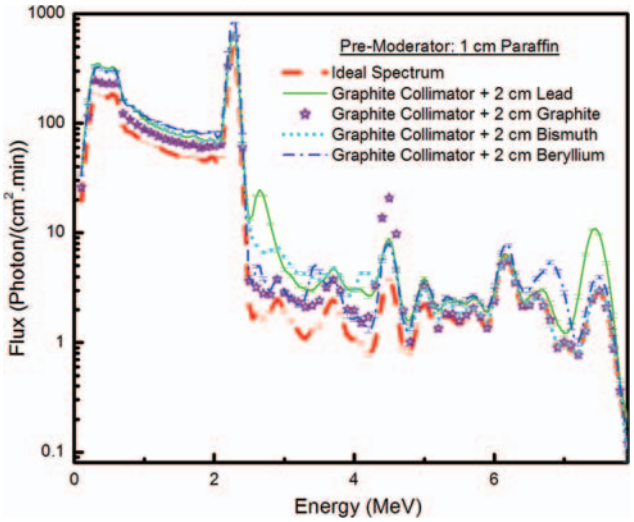

Fig. 5. Detector spectrum using different collimators with the same PM (1.0 cm paraffin).

produced in paraffin slabs (2.23 MeV and 4.43 MeV) do not lie in the chlorine ROI (6 MeV to 8 MeV), due to the great number of photons emitted from the PM, a pulse pile up phenomenon affects the detector spectrum for energies beyond 5 MeV. Two or more photons are detected and (possibly) some deposited energies from them are recorded as a single event. In addition, if a high number of photons are received by the detectors, the lifetime of the detectors is shortened. The aforementioned reasons are alone sufficient to limit the PM thickness to 3 cm, however, the MCNPX code cannot consider them.

In the case of a collimator based upon Tables 5 and 6, adding a Be layer with a thickness of 5 cm to the collimator reduces the CV value and increases the mean value of the activation rate. However, using a Be collimator leads to high background in the detector spectrum in the chlorine ROI (Fig. 5). Moreover, because of the strategic importance of Be to the defense and space industries and its expensive price, using this element as a collimator with such a large volume (97 800 cm^3) is not affordable. Eliminating Be from the options, the best CV values are found with a graphite collimator without a neutron multiplier layer and a Bi collimator.

As shown in Fig. 5, for energies smaller than 4 MeV, all of the obtained spectra are very different from the ideal situation. However, detector spectra of the facilities without a multiplier layer and with a thick Bi layer have a reasonably good fit with the ideal spectra in the chlorine ROI. While, for a similar thickness of paraffin PM, the mean value and sensitivity of the setup with a 2-cm Bi layer on the collimator are higher than in the facility without a multiplier layer. Thus, a collimator with a 2-cm Bi layer is the optimum choice.

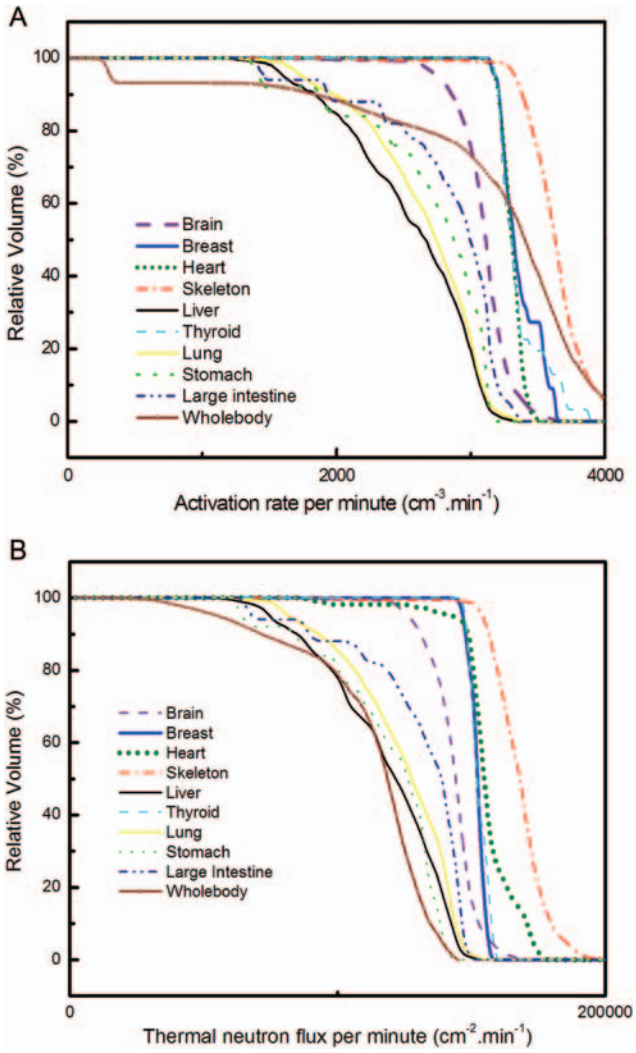

Fig. 6. Activation rate and thermal neutron flux volume histograms of some important organs.

Final facility

A quick comparison of various thicknesses of PM using the selected collimator showed that 3 cm paraffin may be a suitable option. Looking at Table 6, by increasing PM thickness to 1.5 cm the mean value of activation rate increases slightly. But for thicknesses higher than 1.5 cm, the mean value is decreased. Moreover, reductions in the effective dose at the same thicknesses are adequate to increase the sensitivity parameter. Therefore, a paraffin slab with a 3-cm thickness is selected as the final PM.

Figure 6 shows the activation rate and thermal neutron flux cumulative volume histograms. It is observed that the distributions of activation rate and thermal neutron flux are fairly uniform for some organs such as breasts, heart, thyroid, skeleton and brain. In other organs such as lungs, liver and large intestine, which are expanded through the body, the activation rate histograms drop with small slopes.

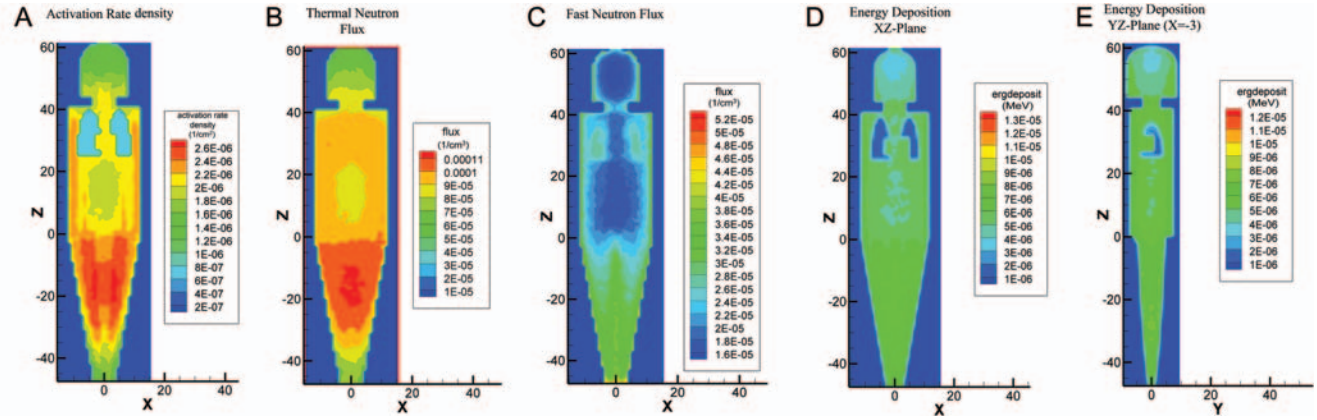

Fig. 7. 2D plot of the activation rate (**A**), thermal neutron flux (**B**), fast neutron flux (**C**) and energy deposition (**D**) in a two-dimensional array at mid-depth of the phantom ($Y = 0$). A YZ-plot of energy deposition (**E**) located in X = –3 cm is also presented.

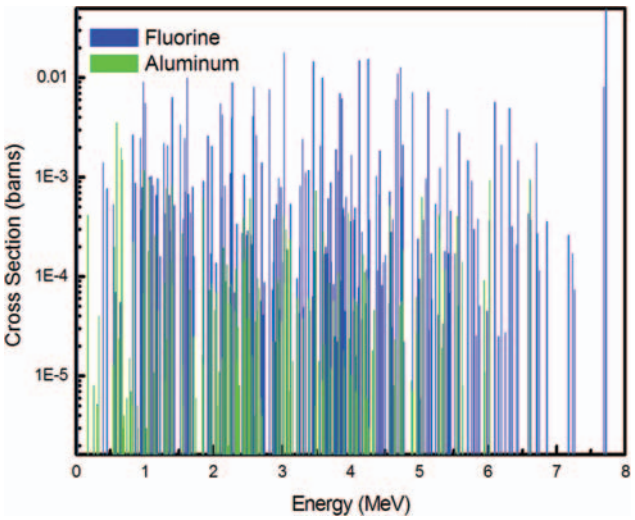

Fig. 8. Prompt gamma neutron activation cross-section in terms of photon energy of Al.

The stomach wall, although it is a relatively small organ, does not have a smooth histogram because of its position in the body. Various parts of the stomach wall are located at different depths of body, so the activation rate is dispersed in this organ.

Figure 7 depicts 2D-plots of activation rate, energy deposition, thermal and fast neutron flux in a two-dimensional array at mid-depth of the phantom. As expected, because of the low density of lung tissue, thermal neutron flux decreases in the lungs. In addition, in the upper part of the head and lower parts of the legs, the activation rate also reduces, due to the relative thinness of tissue in these parts and their increased distances from the sources. In addition to thermal flux, the activation rate is also dependent on the number of nuclei per unit volume. So for similar thermal neutron fluxes, bone tissue would be more activated than soft and lung tissues and the uniformity of activation rate would be reduced. The problem is even more complicated as thermal neutron flux is not uniform enough in the body. Figure 7B shows the reduction of thermal neutron flux in the mid-depth because of the high absorption of thermal neutrons in the media. In the boundary regions thermal fluxes are also low. According to the distribution of fast neutrons, it is apparent that in the surface layer of the body and in the region of the lungs, the moderating process is not intensive. In addition, because of the conical shape of the legs, there is little tissue between the two legs and so fast neutron flux is relatively high in this region. As a consequence, thermal neutron flux is not uniform within the phantom. So, because of the non-uniform distribution of thermal neutron flux and heterogeneities in the human body, activation rates are not adequately uniform. In future work, we will try to find a proper shape for PM, which can at least partly compensate for the effect of the heterogeneity of the phantoms. In Fig. 7D and 7E, the uniform energy deposition distribution can be observed. However, there are some light regions between the legs. These light regions are due to the existence of more fast neutrons in this part. In the head and trunk, fast neutron flux was reduced because of the moderation process at the same depth. So, the delivered dose in these parts was smaller than for the legs.

CONCLUSION

The main goal of this paper was to study the role of the PM and collimator in IVNAA facilities and to design an optimal setup that would reduce the CV of thermal neutron flux and improve activation rate distribution in large biological samples. The activation rate, neutron flux and energy deposition values were calculated in a latticed mathematical human phantom using the MCNPX code. According to the given results, paraffin and water provide

the most uniform distribution among the studied cases. However, paraffin data shows better performance than water results in terms of effective dose and sensitivity. In addition, the PM is more easily constructed with paraffin than with water. So paraffin was selected as the PM material. In the next step, to increase the activation rate in the body, a surface layer of collimator was replaced with a neutron multiplier one. A smaller CV value was obtained using a Bi layer on the collimator and two paraffin slabs with a thickness of 3 cm on the top and bottom of the phantom. The final facility improves the uniformity from 13.9% to 12.7%. Although thick paraffin slabs (10 cm) decreased the CV value to around 10%, it was not a favorable choice owing to detection difficulties. The final setup provided appropriate mean values of activation rate (4.14×10^3 min^{-1}) and sensitivity (3.29×10^{-4} Sv^{-1}) with an adequately small effective dose (12.6 $\mu Sv.min^{-1}$) compared with the other facilities.

FUNDING

This study was supported by a grant from the Ferdowsi University of Mashhad (p/1375-10/12/1387).

ACKNOWLEDGEMENTS

The authors are grateful for the detailed and instructive comments of the journal referees.

REFERENCES

1. Kenneth JE. In vivo neutron activation analysis. In: Aflassi ZB (ed). *Activation Analysis*, 2nd vol.: Boka Raton, Florida: CRC Press, 1990, 407–24.
2. Anderson J, Osborn SB, Tomlinson RWS *et al*. Neutron activation analysis in man in vivo: a new technique in medical investigation. *Lancet* 1964;**2**:1201–5.
3. Chamberlain MJ, Fremlin JH, Peters DK *et al*. Total body calcium by whole body neutron activation: new technique for study of bone disease. *Brit Med* 1968;**2**:581–3.
4. Chettle DR, Fremlin JH. Techniques of in vivo neutron activation analysis. *Phys Med Biol* 1984;**29**:1011–43.
5. Miri Hakimabad H, Rafat Motavalli L. Improving the uniformity of the gamma production rate distribution with depth in a large biological sample for an IVNAA facility. *J Nucl Technol Radiat* 2009;**24**:119–25.
6. Trkov A, Žerovnik G, Snoj L *et al*. On the self-shielding factors in neutron activation analysis. *Nucl Instrum Meth A* 2009;**610**:553–65.
7. Battye CK, Tomlinson RWS, Anderson J *et al*. Experiment relating to whole-body activation analysis in man in vivo using 14-MeV incident neutrons. *Nuclear Activation Techniques in the Life Sciences* 1967;573–82.
8. Palmer HE, Nelp WB, Murano R *et al*. The feasibility of in vivo neutron activation analysis of total body calcium and other elements of body composition. *Phys Med Biol* 1968;**13**:269–79.
9. Nelp WB, Palmer HE, Murano R *et al*. Measurement of total body calcium (bone mass) in vivo with the use of total body neutron activation analysis. *Lab Clin Med* 1970;**76**:151–62.
10. Chamberlain MJ, Fremlin JH, Holloway I *et al*. Use of the cyclotron for whole body neutron activation analysis: theoretical and practical considerations. *Appl Radiat Isot* 1970; **21**:725–34.
11. Cohn SH, Fairchild RG, Shukla KK. Theoretical consideration in the selection of neutron sources for total-body neutron activation analysis. *Phys Med Biol* 1973;**18**:648–57.
12. Stamatelatos IE, Chettle DR, Green S *et al*. Design studies related to an in vivo neutron activation analysis facility for measuring total body nitrogen. *Phys Med Biol* 1992; **37**:1657–74.
13. Stamatelatos IE, Dilmanian FA, Ma R *et al*. Calibration for measuring total body nitrogen with a newly upgraded prompt gamma neutron activation facility. *Phys Med Biol* 1993; **38**:615–26.
14. DJ Borovnicar, Stroud DB, Wahlqvist ML *et al*. A neutron activation analysis facility for in vivo measurement of nitrogen and chlorine in children. *Australas Phys Eng Sci Med* 1996;**19**:252–79.
15. Miri Hakimabad H, Rafat Motavalli L. Investigation of activation rate uniformity in a prompt-γ rays IVNAA facility. *J Radiat Res* 2010;**51**:123–30.
16. McNeill KG, Thomas BJ, Sturtridge WC *et al*. In vivo neutron activation analysis for calcium in man. *J Nucl Med* 1973;**14**:502–6.
17. Rezaei Moghaddam Y, Rafat Motavalli L, Miri Hakimabad H. Shielding optimization in an vivo activation analysis setup. *J Radio anal Nucl Chem* 2012, doi:10.1007/s10967-012-1978-5.
18. Cristy M. Description of the mathematical phantom. *Oak Ridge National Laboratory*, ORNL/TM-8381, 2009.
19. Glasstone S, Sesonke A. Diffusion and slowing down of neutrons. *Nuclear Reactor Engineering*. New York: Van Nostrand Reinhold Company, 1994, 109–47.
20. Catto GRD, McIntosh JAR, Macleod M. Partial body neutron activation analysis in vivo: a new approach to the investigation of metabolic bone disease. *Phys Med Biol* 1973; **18**:508–17.
21. Hendricks JS, Frankle SC, Court JD. ENDF/B-VI Data for MCNPTM, *Los Alamos National Laboratory*, *Report LA-12625*, 1994.
22. Vartsky D, Ellis KJ, Cohn SH. In vivo measurement of body nitrogen by analysis of prompt gammas from neutron capture. *J Nucl Med* 1979;**20**:1158–65.
23. International Atomic Energy Agency. Prompt gamma ray neutron activation analysis. www-nds.iaea.org/pgaa/pgaa7/ (22 May 2012).
24. Kononov V, Kononov O, Soloviev N *et al*. Accelerator based epithermal neutron source for NCT. *International Symposium of Boron Neutron Capture Therapy* 2004;50–61.
25. Blue TE, Yanch JC. Accelerator-based epithrmal neutron sources for boron neutron capture therapy of brain tumors. *J Neuro-Oncol* 2003;**62**:19–31.

26. Bleuel DL, Chu WT, Donahue RJ *et al*. Initial experimental verification of the neutron beam modeling for the LBNL BNCT facility. *15th International Conference on the Application of Accelerators, in Research and Industry*, 1999.
27. Cristy M, Eckerman K. Specific absorbed fractions of energy at various ages from internal photon sources. *Oak Ridge National Laboratory*, ORNL/TM-8381N1, 1987.
28. Snyder W, Ford M, Warner G *et al*. Estimate of absorbed fractions for monoenergetic photon source uniformly distributed in various organs of a heterogeneous phantom Medical Internal Radiation Dose Committee (MIRD) Pamphlet No. 5 Revised, New York: The Society of Nuclear Medicine, 1987.
29. Han EY, Bolch WE, Eckerman KF. Revision to the ORNL series of adult and pediatric computational phantoms for use with the MIRD schema. *Health Phys* 2006;**90**:337–56.
30. Ulanovsky AV, Eckerman KF. Absorbed fractions for electron and photon emission in the developing thyroid fetus to five year old. *Radiat Prot Dosim* 1998;**79**:419–23.
31. Knoll GF. Radiation interactions. In: *Radiation Detection and Measurement*, 4th ed. John Wiley & Sons, 2010, 54–55.
32. Drzymala RE, Mohan R, Brewster L *et al*. Dose volume histograms. *Intl J Rad Oncology, Biology and Physics* 1991;**21**:71–8.
33. Nioutsikou E, Webb S, Panakis N *et al*. Reconsidering the definition of a dose-volume histogram. *Phys Med Biol* 2005;**50**:L17–L19.
34. International Commission on Radiological Protection. The 2007 Recommendations of the International Commission on Radiological Protection. ICRP Publication 103. Ann. ICRP 37 (2–4), 2007.
35. National Council on Radiation Protection and Measurements. Protection against Neutron Radiation. *NCRP Report No. 38* (Bethesda, MD: NCRP), 1971.
36. Waters L. MCNPXTM user's manual, version 2.4.0. Report LACP-02-408, *Los Alamos National Laboratory*, 2002.
37. Kluge H, Weise K. The neutron energy spectrum of a 241Am-Be(Alpha, n) source and resulting mean fluence to dose equivalent conversion factors. *Radiat Protect Dosim* 1982;**2**:85–93.
38. Miri Hakimabad H, Panjeh H, Vejdani Noghreiyan A. Evaluation the nonlinear response function of a 3×3 in NaI scintillation detector for PGNAA applications. *Appl Radiat and Isot* 2007;**65**:918–26.
39. Croft S. The use of neutron intensity calibrated 9Be (alpha,n) sources as 4438 KeV g-ray reference standards. *Nucl Instrum Meth A* 1989;**281**:103–16.
40. Briesmeister JF, MCNP 4C General Monte Carlo n-particle transport code. *Version 4C. Report LA-13709-M*, *Los Alamos National Laboratory*, 2000.